J. S. Afr. Inst. Min. Metall., vol. 89, no. 8.
Aug. 1989. pp. 243-249.

Properties of laser-welded and electron-beam-welded ferritic stainless steel

by M. TULLMIN*, F.P.A. ROBINSON*, C.A.O. HENNINGt, A. STRAUSSt, and J. LE GRANGEt

SYNOPSIS

An experimental ferritic stainless steel with a chromium content of 40 per cent was welded by laser and electron-beam (EB) welding processes. These techniques were found to be particularly suited to the welding of this alloy in that the impact toughness of the weld metal and heat-affected zone (HAZ) of the laser welds compared favourably with those of the parent alloy. When the EB process was used, the impact toughness of the weld metal was over 180 J/cm^2. Grain growth in the HAZ was minimal for welding with these two processes. Corrosion tests, conducted in a solution consisting of 20 per cent sulphuric acid and 100 p.p.m. of potassium thiocyanate, and in a highly corrosive industrial solution, indicated that the laser and EB welds were free of sensitization effects, thus confirming the metallographic results.

SAMEVATTING

'n Eksperimentele ferritiese vlekvrye staal met 'n chroominhoud van 40 persent is volgens die laser- en elektronebundelsweisproses gesweis. Daar is gevind dat hierdie tegnieke besonder geskik vir die sweis van hierdie legering is aangesien die slagtaaiheid van die sweismetaal en hitte-invloedsone van die lasersweislasse gunstig met dié van die basislegering vergelyk het. Toe die elektronebundelproses gebruik is, was die slagtaaiheid van die sweismetaal meer as 180 J/cm^2. Korrelgroei in die hitte-invloedsone was minimaal vir sweiswerk volgens hierdie twee prosesse. Korrosietoetse wat uitgevoer is in 'n oplossing bestaande uit 20 persent swaelsuur en 100 d.p.m. kaliumtiosianaat, en in 'n hoogs korroderende industriële oplossing, het getoon dat laser- en elektronebundel-sweislasse vry van sensitiseringseffekte was wat die metallografiese resultate bevestig.

Introduction

Extensive research has taken place during the past two decades in the field of high-chromium ferritic stainless steels. The major advantages of these alloys over the austenitic grades are their resistance to chloride stress-corrosion cracking, and the lower cost resulting from their low nickel contents. However, ferritic stainless steels have been used far less extensively than the austenitic alloys. This limited use of ferritic grades stems from their generally low toughness, and also poor weldability, particularly in thicker sections.

By the 1950s, it had already been established that the poor toughness of ferritic stainless steels is related to the levels of carbon and nickel in these steels, rather than to their high chromium contents. Renewed interest in the ferritic stainless alloys coincided with the introduction of modern refining techniques for stainless steels, such as vacuum-oxygen decarburization and electron-beam hearth refining. The recently developed ferritic stainless alloys, termed ELI (extra-low interstitial) or super ferritic stainless steels, are characterized by superior toughness, intergranular corrosion resistance, and weldability over those of the earlier grades.

The development of the new high-chromium ELI stainless steels has concentrated on a chromium range of 25 to 30 per cent, with no commercial alloys having chromium contents in excess of 32 per cent[1]. The main problem with higher chromium contents is that the requirements for low levels of carbon plus nickel become more critical as the chromium content increases. However, corrosion studies have indicated that the optimum passivation characteristics of iron-chromium alloys and iron-chromium alloys with alloying additions of platinum-group metals (PGM) occur at a level of 40 per cent chromium[2,3].

In view of these findings, a number of research projects on the properties of Fe-40Cr alloys have been initiated by Mintek. Relatively tough experimental Fe-40Cr alloys have been produced in South Africa[4-6] in the annealed condition. The study described here set out to establish the weldability of an experimental Fe-40Cr ferritic stainless steel welded by use of the laser and electron-beam (EB) processes. Laser welding, in particular, has undergone widespread growth and has now become a well-established industrial process in Europe and the USA.

A fully automated facility with industrial-scale laser and EB welding workstations is available in South Africa, although these two processes can be regarded as relatively new and not well-known to the local industry. Laser and EB welding are particularly suited to Fe-40Cr alloys because the heat input is considerably lower than in arc processes. Compared with TIG welding using about 150 J/mm^2 of joint area, a typical value for laser and EB welding is only 20 J/mm^2. It is usually desirable to weld ferritic stainless steels with a minimum heat input to avoid severe grain growth and embrittlement in the heat-affected zone (HAZ). Additional advantages of laser and EB welding are that no electrode or filler is required, weld contamination is extremely low, the HAZ and the weld are extremely narrow and hence, compared with arc welding, the residual stresses are very low. The laser and

* Department of Metallurgy and Materials Engineering, University of the Witwatersrand, P.O. 2050, Johannesburg 2000.
† HTP Marketing & Manufacturing, P.O. Box 19823, Pretoria 0117.

ISSN 0038-223X/3.00 + 0.00. Paper received 20th March, 1989.

EB weldments in the experimental Fe–40Cr alloy were tested for corrosion resistance and impact toughness. Metallographic microstructural analysis was also undertaken.

Alloy Composition and Processing Route

The chemical composition of the experimental Fe-40Cr alloy used in the welding studies is presented in Table I. Vacuum-induction melting and the use of raw materials of the highest purity ensured that the carbon and nickel contents were extremely low, at 0,003 and 0,055 per cent respectively.

TABLE I
CHEMICAL COMPOSITION OF THE EXPERIMENTAL Fe–40Cr ALLOY
(All values in percentages by mass)

C	0,003	Mo	2,13
N	0,0055	Cr	38,64
S	0,007	Ni	2,08
P	0,006	Nb	0,14
Mn	0,01	V	0,19
Si	0,02	Al	0,2
Cu	0,47	Fe	Balance

It has been established that susceptibility to intergranular corrosion can still occur in annealed Fe–40Cr alloys despite the extremely low interstitial levels[7]. To overcome this problem, niobium was added to the alloy to tie up the carbon and nickel in the form of stable niobium–carbonitrides. Molybdenum and nickel were added to the alloy for enhanced resistance to pitting corrosion and improved toughness respectively. Copper, vanadium, and aluminium additions were included as 'weld ductilizers', and have been shown to lead to improved weld ductility in high-chromium ferritic stainless steels at the concentration levels used in this alloy[8].

The Fe–40Cr alloy was hot-rolled down to 7 mm thick plate. Subsequent to rolling, the alloy was annealed at 850°C for 1 hour and then allowed to cool in air. The final annealing heat treatment was at 1050°C for 1 hour, followed by quenching in brine cooled with dry ice. The purpose of the rapid quench is to prevent the precipitation of chromium–carbonitride, which is deleterious to the steel. This two-stage annealing cycle has been established as a means of achieving 'optimum' toughness in this type of alloy.

Laser- and EB-welding Parameters

The Fe–40Cr alloy was welded with a 2,2 kW carbon dioxide laser. The welds were made by the joining together of two 6 mm plates by a close square-butt joint technique. The edges of the plates were pushed together and held in place on the magnetic base of an NC table during welding. The laser used represents the maximum laser power available in South Africa, but ideal power requirements for the welding of 6 mm plate are higher, at about 5 kW. Owing to the limited power available, the weld runs had to be carried out from opposite sides to obtain complete penetration. The following laser-welding parameters were used:

Laser power	2,00–2,05 kW
Focal point	2 mm inside workpiece
Welding speed	0,6 or 1 m/min
Shielding gas	Pure helium
Welding-nozzle diameter	3,3 mm.

Because of power constraints, the focal point had to be maintained well inside the workpiece. This represents usual laser-welding practice, but the optimum focal position in 6 mm steel plates has been established as being 1 mm inside the workpiece[9]. This position would probably result in slightly wider weld-bead formation, making alignment easier. The welding speed was maintained at a minimum of 0,6 m/min. At lower speeds, the profile of the laser weld tended to be relatively wide (U-shaped), without the characteristic narrow keyhole formation. To limit the formation of plasma above the weld pool, pure helium was used as the shielding gas throughout, with a welding nozzle of 3,3 mm diameter. Argon, which has a lower ionization potential than helium, is more prone to plasma formation above the weld pool[9]. Plasma formation is highly undesirable, since it tends to deflect the laser beam, reducing the depth of penetration. The welding nozzle used produced a relatively wide shielding envelope round the weld.

The nature of the EB process is in many ways very similar to laser welding, with a characteristic 'keyhole' type of weld pool. However, since this process is carried out under vacuum, there is no need for a shielding gas, and there are therefore no problems of plasma formation. At an equivalent power input, deeper penetration levels are thus attainable in EB welding. It is often suggested that the laser and EB processes are interchangeable. In view of the higher power available and the higher inherent penetration of the EB process, full penetration welds were made in 6 mm thick Fe–40Cr alloys by welding only from one side with the following parameters:

Potential	120 kV
Current	28,5 mA
Focal current	17,14 mA
Welding speed	1,5 m/min.

Figs. 1 and 2 show typical macrostructures of the laser and EB welds.

Microstructure of the Laser and EB Weldments

Specimens were sectioned parallel to the welding direction and were prepared by standard metallographic techniques. The etching was done electrolytically in oxalic acid at a current density of 0,5 A/cm^2.

The microstructure of the laser-weld metal consisted largely of columnar grains formed by epitaxial growth, as shown in Fig.3. The strong epitaxial character of the solidification stems from the steep temperature gradients associated with laser welding (typically[10] 10^5 C/cm). Because of the steep temperature gradients, only a very thin chilled layer tends to be sufficiently cool to solidify. In most alloys, grains from the substrate grow into the chilled zone, and grains nucleated in the weld pool redissolve or are transported ahead of the melt front[10]. In general, the columnar grains of the weld metal tended to be somewhat coarser than the grains in the parent plate. This phenomenon is related to the preferential growth of certain grains oriented in fast-growing directions (100 for cubic crystals). Epitaxial solidification thus tends to produce coarsening and preferred crystallographic texture in the microstructure.

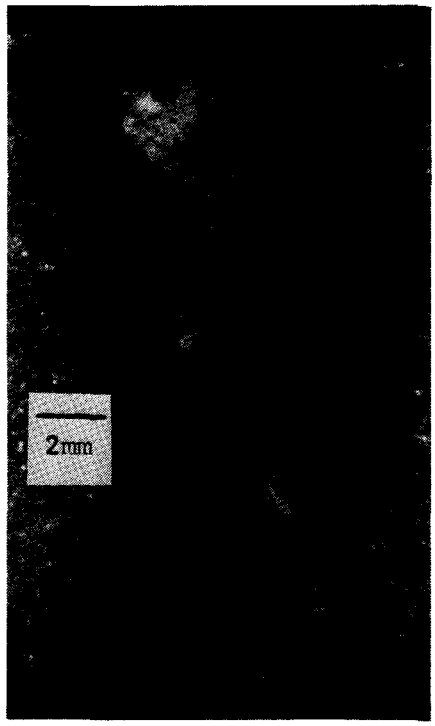

Fig. 1—Macrostructure typical of laser welds

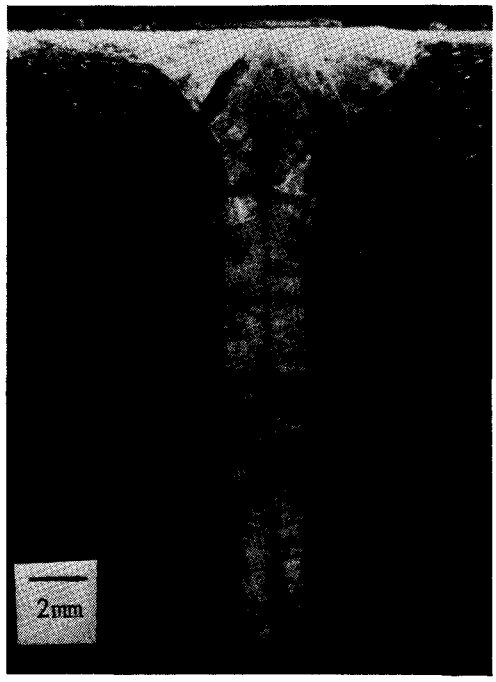

Fig. 2—Macrostructure typical of EB welds

The dendritic character of the weld-metal grains is evident in the microstructure shown in Fig. 4. During the solidification process, there is usually a partitioning of solute atoms ahead of the solid–liquid interface. This partitioning tends to produce geometric instabilities, resulting in dendritic solidification. The high temperature gradients and cooling rates associated with laser welding minimize the extent of segregation because of the short times available for lateral diffusion[10]. Along the centre line of the laser welds, a relatively narrow zone of finer equiaxed grains was found, mainly at the base of the 'keyhole'. These finer grains probably originally nucleated in the molten zone, and were transported ahead of the solidification fronts until these fronts eventually met.

No evidence of sensitization was detected in either the weld metals or the HAZs of the laser welds. The weld-metal grains shown in Fig. 4 were free of grain-boundary precipitates with a step-like structure. The shielding method used in the laser welding thus appears to have been particularly effective. Another characteristic feature of the laser welds was the virtual absence of grain growth in the HAZ. This phenomenon, illustrated in Fig. 5, is related to the relatively low heat input associated with laser welding. The fine dispersion of niobium–carbonitrides in the alloy is also expected to exert pinning effects on grain boundaries.

The microstructure of the EB welds was very similar in nature to that described above for the laser welds. The EB-weld metal also consisted mainly of columnar grains formed by epitaxial growth, with a fine equiaxed zone along the centre line. The grains were free of grain-boundary chromium–carbonitride precipitates, as shown in Fig. 6, and somewhat coarser than the grains in the parent plate. There was no significant grain coarsening in the HAZ of the EB welds, for reasons similar to those described for the laser welds.

Impact Toughness of the Laser and EB Weldments

Charpy impact tests in 5 mm thick specimens were conducted at room temperature, with notches located in the weld metals and HAZs of the Fe–40Cr alloy. Notching in the weld metal posed no problems, the remelted zones being wide enough to contain the crack path in the weld metals. The machining of reproducible notches in the HAZ of welds is considered more difficult. The different HAZ regions exhibit different properties, and it is extremely difficult to machine a notch repeatedly at the same HAZ location. For this reason, weld simulation of HAZ thermal cycles in arc welding is often undertaken on Charpy specimens. Unfortunately, weld simulators do not provide sufficiently fast cooling rates to simulate laser or EB thermal cycles. Thus, testing has to be performed on the actual HAZ of weld specimens. An advantageous feature of laser and EB weldments is that the HAZ is relatively straight, so that the crack path is confined to a relatively uniform HAZ structure. In the present study, the Charpy V-notches were all placed within a strip 1 mm away from the fusion boundary. From the heat tint produced on laser welds in air, the actual HAZ width was estimated to be about 2 mm. When similar laser powers were used in the welding of titanium alloys, a HAZ width of about 3 mm was found, with a minimum temperature of around 720°C in the HAZ[11].

The average Charpy-impact energies of the laser- and EB-weld zones are listed in Table II. At both welding speeds, the impact toughnesses of the laser-weld metal and HAZ were higher than that of the parent alloy. The fracture surfaces of the weld metal and HAZ exhibited extensive plastic deformation, with an associated ductile dimpled fracture mechanism at the edges of the specimen. The centre of the specimen fractured in a mixed mode—transgranular cleavage combined with dimpled regions. These two distinct zones naturally arise from the different

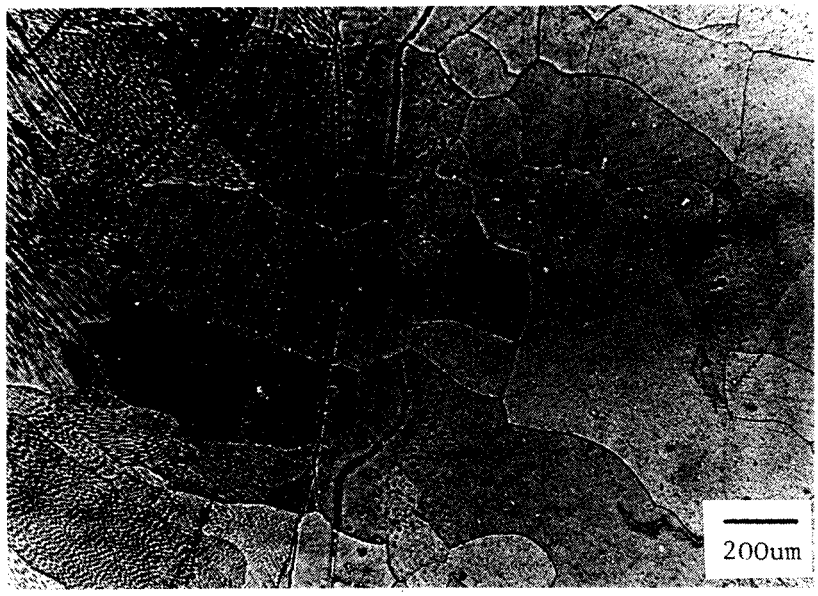

Fig. 3—Microstructure of the laser weld at the fusion boundary

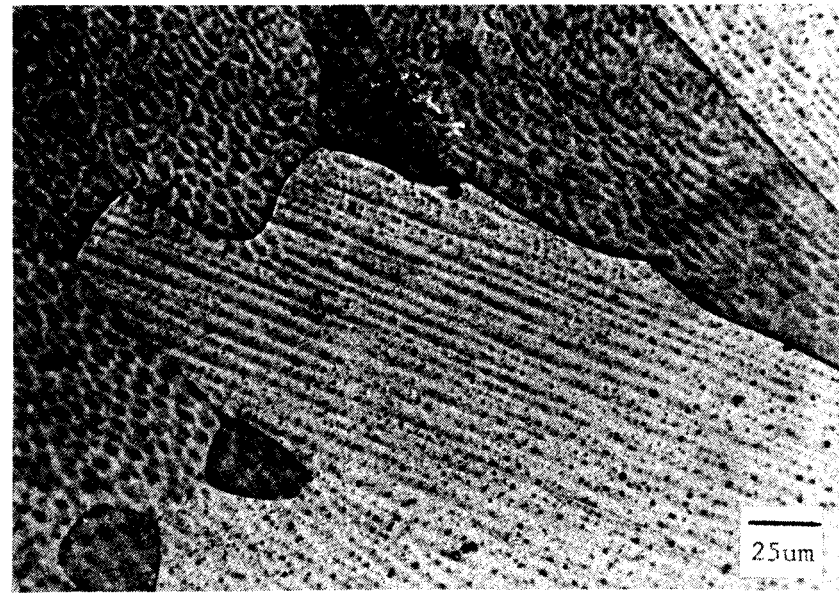

Fig. 4—Microstructure of laser-weld metal

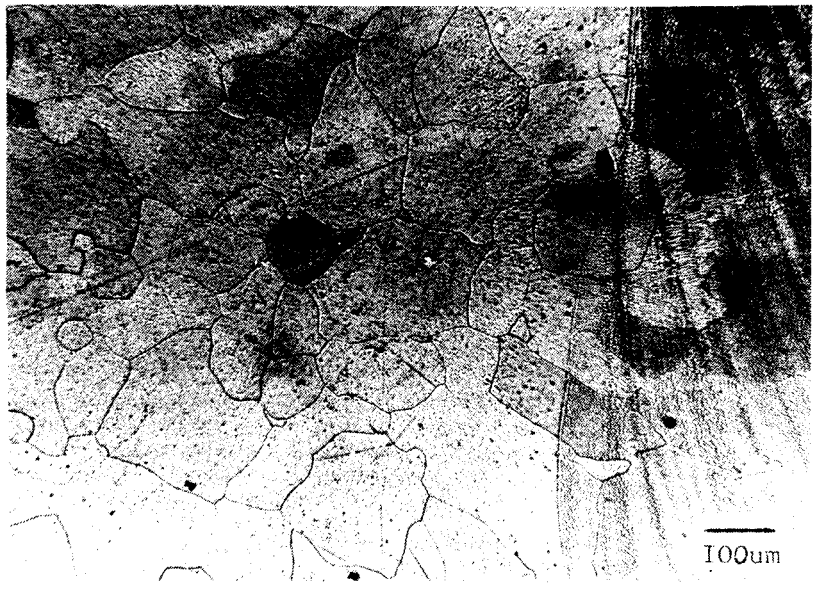

Fig. 5—Laser-weld microstructure showing grain size in the HAZ

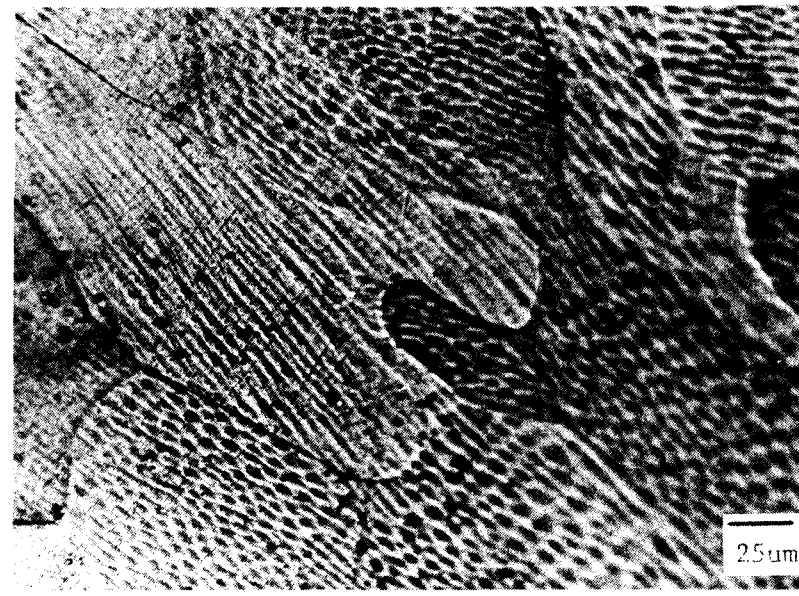

Fig. 6—Microstructure of the EB-weld metal

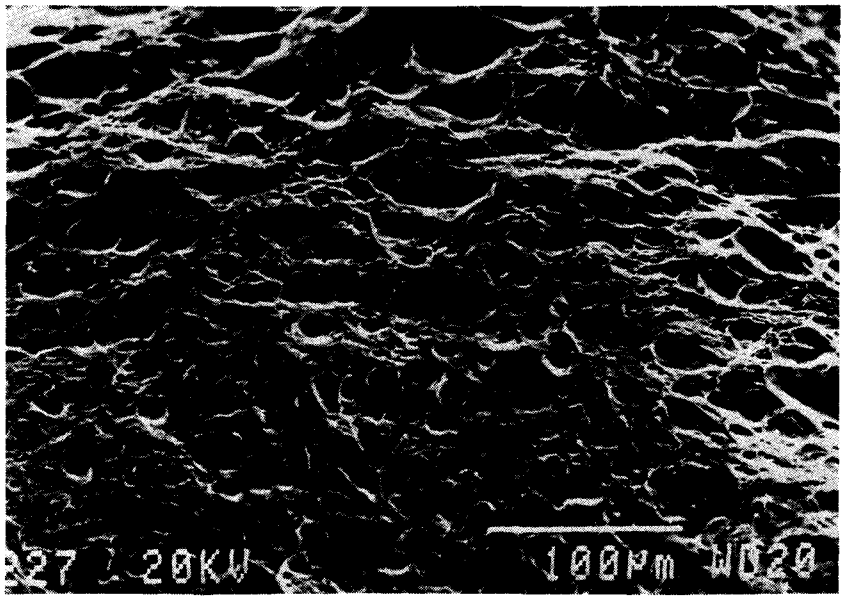

(a)

Fig. 7—Fracture appearance of the laser-weld metal
(a) Ductile rupture at shear lips near the specimen edges
(b) Mixed-mode fracture with cleavage patterns near the centre of the specimen

(b)

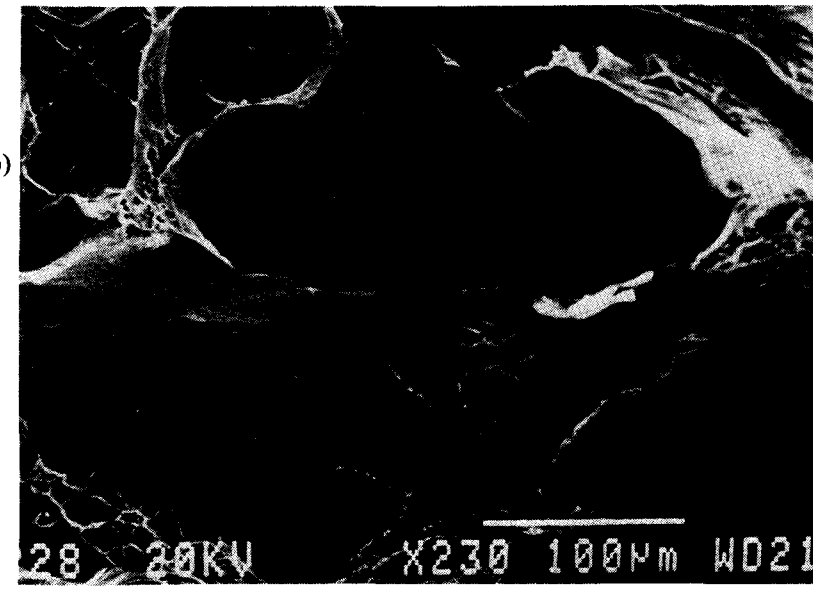

degrees of plastic constraint at the edges of the specimen compared with the centre. The microscopic fracture modes as examined by scanning electron microscopy (SEM) are illustrated in Fig. 7.

TABLE II
IMPACT ENERGIES OF THE LASER AND EB WELDMENTS

Weldment	Impact energy, J/cm²		
	Weld metal	HAZ	Parent plate
Laser (1 m/min)	52	42	41
Laser (0,6 m/min)	52	68	41
EB (1,5 m/min)	184	44	41

The EB-weld metal of the Fe–40Cr alloy displayed a remarkably high toughness of over 180 J/cm². These results are in good agreement with the Charpy impact data of EB-weld metals published for a high-chromium ferritic stainless steel[12]. It should be borne in mind that ferritic stainless steels characteristically display relatively sharp impact transition temperatures. The high difference in impact energy between the EB-weld metal and the parent plate of the Fe–40Cr alloy may thus be related to a smaller shift in the magnitude of the impact transition temperatures. The HAZ toughness of the EB weldment was found to be very similar to that of the laser HAZ, and only marginally higher than in the parent plate.

The microscopic fracture mode of the EB-weld metal and HAZ was of the same nature as described for the laser weldments. The higher impact energy of the EB-weld metal could be correlated with a higher proportion of ductile dimpled rupture.

Corrosion Resistance of the Laser and EB Weldments

The corrosion resistance of the Fe–40Cr welds was assessed by accelerated electrochemical corrosion tests. The potentiodynamic polarization studies were conducted in two media:

(1) de-aerated 20 per cent (by volume) H_2SO_4 + 100 p.p.m. of KSCN at 40°C and
(2) aerated Mhlatuze effluent solution at 50°C.

The sulphuric acid solution was used for an assessment of the general corrosion resistance of the different weld zones, and KSCN was added to this solution to stimulate intergranular dissolution in the event of sensitization. Sensitized Fe–40Cr alloys have been observed to effectively disintegrate in this medium, with associated extremely high corrosion rates[13]. At a chloride level of 24 000 p.p.m. and a pH value of 1,4, the Mhlatuze effluent must be regarded as extremely corrosive. Pitting is the expected dominant form of corrosion in this medium. When the weld metals and HAZs were tested, the remaining specimen areas were masked off with corrosion-resistant lacquer. In this way, the HAZ was evaluated over a width extending 1 mm away from the fusion boundary.

In solution (1), the laser- and EB-weld metal and HAZ were found to have polarization curves that were virtually identical to those for the parent Fe–40Cr alloy, an example of which is shown in Fig. 8. The corrosion rates are listed in Table III. The critical current densities followed similar trends, and the E_{corr} values of the different weld zones were all around −420 mV. There were no significant differences in the corrosion rates between the laser- and the EB-weld metals and HAZs. These corrosion rates were somewhat higher than those of the parent plate, but two orders of magnitude lower than those for sensitized Fe–40Cr material. It was concluded that the laser and EB weldments were free of sensitization effects and exhibited a relatively high degree of corrosion resistance. SEM examination confirmed the absence of any intergranular corrosion penetration in either the weld metals or the HAZs.

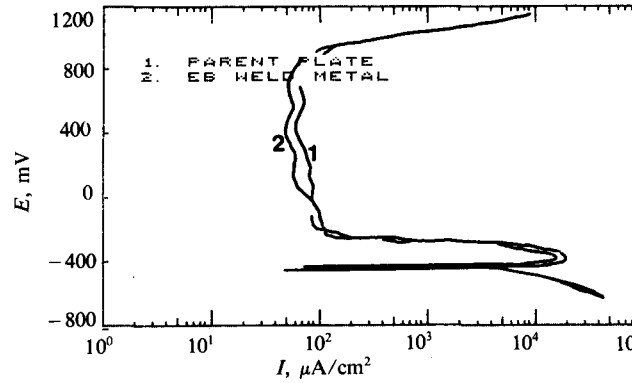

Fig. 8—Potentiodynamic polarization curves in solution (1)

TABLE III
CORROSION RATES OF LASER AND EB WELDMENTS IN SOLUTION (1) AT 40°C

Weldment	Corrosion rate, mpy		
	Weld metal	HAZ	Parent plate
Laser (1 m/min)	780	690	370
EB (1,5 m/min)	596	617	370
Sensitized Fe–40Cr alloys			26000–99000

Similar corrosion-resistance characteristics were observed for the laser and EB welds in the Mhlatuze effluent — solution (2). All the weld zones displayed extensive passive ranges and relatively high pitting potentials, which are listed in Table IV. The pitting potentials of the parent plate and the weld zones were all within 20 mV of one another, i.e. within the limits of experimental accuracy. Pit initiation in the laser- and EB-weld metals and HAZs occurred randomly at sulphur- and silicon-rich inclusions. The pitting results thus confirm the relatively high degree of corrosion resistance of the laser and EB weldments, and also the absence of any sensitization effects.

TABLE IV
PITTING POTENTIALS IN MHLATUZE EFFLUENT

Weldment	Pitting potential, mV vs SCE		
	Weld metal	HAZ	Parent plate
Laser (1 m/min)	840	850	860
EB (1,5 m/min)	860	840	860
Sensitized Fe–40Cr alloys			<200

Discussion of Results

The results of the weldability studies indicated that the laser and EB processes are particularly suited to the welding of Fe–40Cr ferritic stainless steel. The impact toughness of the HAZs and weld metals associated with these two welding techniques compared very favourably with that of the parent alloy. The toughness of Fe–40Cr alloys is a complex function of grain size, morphology and distribution of precipitates, mobile dislocation density[6], interstitial content, and concentration of alloying elements.

The grain size in the HAZ of the laser and EB welds was found to be very similar to that of the parent plate. The problem of extensive grain coarsening and associated brittleness often cited in the welding of ferritic stainless steels by arc processes is essentially absent from laser and EB processes. The grain sizes of the laser- and EB-weld metals were marginally coarser than those of the parent plates as a result of characteristic epitaxial solidification. Additional grain-refinement techniques in the parent plates would thus be necessary to significantly refine the grain size of the weld metals. However, the laser- and EB-weld metals are expected to be much finer than those of autogenous or matching filler TIG welds.

Owing to the extremely high cooling rates and minimal contamination associated with laser and EB welds, it can be expected that embrittlement resulting from time-dependent precipitation reactions will be minimized. The cooling rates in the weld metals associated with laser and EB processes are as high[10] as 10^7°C/s. The high cooling rates minimize the time that the weld metal remains in the molten state, where interstitial pick-up is most likely. Naturally, the vacuum conditions of the EB process essentially eliminate contamination effects, while the inert shielding gas in laser welding also excludes interstitial elements. A common embrittlement process associated with ferritic stainless steels, especially during welding, is high-temperature embrittlement. This form of embrittlement is related to the inter- and intra-granular precipitation of chromium–carbides and chromium–nitrides during cooling from high temperatures[14]. Intragranular precipitates have been shown to lead to embrittlement by the mechanism of dislocation locking, by which plastic flow is retarded and cleavage enhanced[15]. Intergranular chromium and interstitial-rich precipitates tend to act as cleavage initiation sites, similar to most second phases in ferritic stainless steels.

It has been demonstrated[6] that mobile dislocations enhancing toughness can be generated in Fe–40Cr alloys owing to the differential thermal expansion characteristics between precipitates such as chromium–sulphides and the alloy matrix. Such events may also have contributed to the relatively high toughness of the laser and EB weldments.

In ferritic stainless steels, adequate toughness and corrosion resistance are often closely related. Loss of corrosion resistance in the weld metal and HAZ usually results from grain-boundary chromium–carbonitride precipitates, which also have a detrimental effect on toughness. These grain-boundary precipitates form on cooling through the temperature range 800 to 500°C. A chromium-depleted zone is formed adjacent to these chromium-rich precipitates, leading to poor corrosion resistance in concentrated acid media, particularly pitting corrosion. High-chromium ferritic stainless steels are particularly susceptible to sensitization because the interstitial solubility decreases significantly with increasing chromium content, and is much lower in ferrite than in austenite. The corrosion resistance of the HAZs and weld metals of both the laser and the EB weldments was remarkably high in the extremely corrosive test media, and essentially identical to that of the parent alloy. It is thus apparent that the laser and EB weldments were entirely free of sensitization effects, which was confirmed by microstructural analysis. The high degree of corrosion resistance of the laser and EB weldments can thus be attributed to minimal contamination by interstitial elements and rapid cooling rates. The use of niobium stabilization to combine with these interstitial elements in the form of stable niobium–carbonitrides is an additional contributing factor.

Conclusions

This study showed that high-chromium ferritic stainless steel can be welded successfully by the laser and EB processes. The weldments retained the excellent corrosion resistance and adequate impact toughness of the Fe–40Cr parent plate. Laser and EB welding appear to be particularly suited to alloys relying on minimal contamination by interstitial elements for good toughness and corrosion-resistant properties. Many highly alloyed materials, such as nickel-based alloys and stainless steels, fall into this category. An added advantage of laser and EB welding is that no separate filler materials are required for joining purposes.

Acknowledgements

The authors thank Mintek and the University of the Witwatersrand for permission to publish this paper. Financial assistance from Mintek, the use of welding facilities at High Technology Products, and the technical assistance of Mr Ben Ensslin are gratefully acknowledged.

References

1. BAVAY, J.C., *et al.* Corrosion 87, Paper no. 350. Houston (USA), NACE, Mar. 1987.
2. TOMASHOV, N.D., and CHERNOVA, G.P. *Protection of metals,* vol. 11. 1975. pp. 379–384.
3. CHERNOVA, G.P., *et al. Corrosion,* vol. 34. 1978. pp. 445–448.
4. DEMARSH, E.A. A study of the embrittlement and toughening of Fe–40Cr alloys. M.Sc. dissertation, University of the Witwatersrand, Johannesburg, 1986.
5. HERMANUS, M.A. Development of a tough, high chromium ferritic stainless steel. M.Sc. dissertation, University of the Witwatersrand, Johannesburg, 1986.
6. WOLFF, I.M. Unpublished research, University of Cape Town.
7. TULLMIN, M., *et al. EMSSA*, vol. 18. 1988. pp. 183–184.
8. DEMO, J.J. *Met. Trans.,* vol. 5, Nov. 1974. pp. 2253–2256.
9. MAZUMDER, J. *Laser materials processing.* Amsterdam, North Holland Publishing Co., 1983.
10. *Metals handbook.* 9th ed. Metals Park (USA), ASM, 1987. vol. 13.
11. MAZUMDER, J., and STEEN, W.M. *Met. Trans.,* vol. 13A. May 1982. pp. 865–871.
12. HONEYCOMBE, J., and GOOCH, T.G. *Weldability of stress corrosion resistant stainless steels: Toughness properties.* The Welding Institute, 1975.
13. TULLMIN, M. Unpublished research, University of the Witwatersrand.
14. SEMCHYSNEN, M., *et al.* Towards improved ductility and toughness. *Proc. Conf., Kyoto International Conference Hall, Oct. 1971.* pp. 239–253.
15. DEMO, J.J. *Corrosion,* vol. 27, no. 12. Dec. 1971. p. 531.